Experimental Investigation of Electron Energy Spectra in Collector Region of Moderate-Power Millimeter-Wave Gyrotron

D. Kas'yanenko, O. Louksha and G. Sominski, Saint-Petersburg State Polytechnical University, Russia
B. Piosczyk and M. Thumm, Forschungszentrum Karlsruhe, Institut für Hochleistungsimpuls- und Mikrowellentechnik (IHM), Germany

Abstract

An analyzer with relative energy resolution $\delta\varepsilon_{rms}$ = 0.1 – 0.15 % has been designed for measuring electron energy distribution in a gyrotron collector region. In the 74.2 GHz moderate-power pulse gyrotron, electron energy spectra are studied experimentally in wide ranges of accelerating voltage, beam current and magnetic field values. Influence of RF-fields in the electron beam tunnel, including the fields caused by low-frequency parasitic oscillations, on electron energy spread is determined. Excitation and development of space-charge oscillations in the trap of the gyrotron as well as accompanying changes of energy distribution are calculated numerically. Comparison of experimental results with simulations allows to obtain additional information on collective processes in electron space charge of gyrotron systems.

1 Introduction

To achieve high performance efficiency of a gyrotron, a high quality helical electron beam (HEB) is required. One of the most important quality parameters is the beam energy spread. Even the spread of a few percents can greatly reduce gyrotron efficiency [1,2]. The largest contribution to the spread value at the resonator entrance is attributed to the effect of RF-fields existing in the electron beam tunnel due to various types of instabilities. Well-studied is the instability due to space charge accumulated in the trap between the gun and the resonator as a result of reflection of electrons from magnetic mirror. This instability is accompanied by parasitic low-frequency oscillations (LFO) at frequencies close to 100 MHz [3-5]. In a number of gyrotron experiments, radiation at frequencies up to 1500 MHz was detected also. In [6], authors studied parasitic space-charge oscillations at 900 and 1350 MHz and demonstrated that nature of these oscillations is different from LFO. As regards the RF-fields at the cyclotron frequency, there are basically two mechanisms responsible for such fields: the negative-mass (electrostatic cyclotron) instability and the electron cyclotron maser instability [5,7-10]. If the latter develops in the magnetic compression region, the beam tunnel acts as a resonator. By now, comparative influence of mentioned instabilities on electron energy distribution hasn't been studied, although such information is important for gyrotron improvement.

In an operating gyrotron, direct measurement of the electron energy distribution in the drift region before the resonator without strong disturbing effect on beam characteristics represents a difficult problem. A solution might consist in measurement of electron energy spectra in the collector region [11,12] with subsequent account of strong additional action of resonator fields at the output frequency. In the presence of output radiation, the energy distribution measured in the collector region is formed mostly by resonator fields (and is interesting, in particular, for depressed-collector system design). Yet, such measurement may give helpful information about electron beam characteristics at the resonator entrance as well, if a method to prevent excitation of gyrotron modes is realized.

The report presents new data on electron energy distributions measured in the experimental gyrotron at St.-Petersburg State Polytechnical University. Special attention is given to influence of parasitic low-frequency oscillations on energy spread. Experimental data are compared with the results of calculations simulating changes in energy spectra caused by various types of RF-fields in the gyrotron.

2 Experimental Setup and Measuring Procedure

The measurements have been performed with the experimental gyrotron described in [3]. This tube is equipped with a room-temperature pulse magnetic system and operates in the regime of 30 – 60 μs single pulses. The main geometrical and operating-regime parameters of the gyrotron are summarized in **Table 1**. The maximum output power measured calorimetrically in the operating regime is near 60 kW. In the experiments, we used both the standard geometry of the tube with high Q-factor resonator situated in the plateau region of magnetic field distribution and modified geometries of the gyrotron. In one of the modified versions, the resonator was removed. Around the elec-

tron beam a tube with constant diameter remained. In the other version the resonator was replaced by a special graphite RF-absorber with increasing diameter towards the collector. These modifications served to prevent excitation of gyrotron modes and to distinguish effects of space-charge oscillations on the electron energy distribution.

Accelerating voltage	U_0 = 30 kV
Beam current	I_b = 10 A
Pulse duration	τ = 30 – 60 μs
Cavity magnetic field	B_0 = 2.75 T
Cathode magnetic field	B_c = 0.152 T
Operating mode	$TE_{12.3}$
Operating frequency	f_0 = 74.2 GHz
Cavity radius	R_0 = 14.45 mm
Cavity average beam radius	R_b = 8.43 mm
Cathode average radius	R_c = 35 mm
Cathode angle	$\phi_c = 35^o$
Pitch-factor	α = 1.28

Table 1 Main geometrical and operating-regime parameters of the experimental gyrotron.

For registration of low-frequency instabilities in the HEB and parasitic low-frequency oscillations outside the tube, probes of two types were used [3]. The probe placed in the magnetic compression region measured induced signals from the electron beam near-zone. The external removable antenna was used for measurement of the radiation penetrating outside from the gyrotron through non-metallic details of the tube and external circuits. The apparatus was adjusted for registration of low-frequency signals in the frequency range between 10 MHz and 300 MHz.
It was possible to modify the spatial distribution of the magnetic field in the compression region with a control coil. This technique and the results on parasitic LFO suppression caused by modification of magnetic field distribution were described in [13].

2.1 Electron Energy Analyzer Design

As it was in [11,12], the electron energy analyzer is situated in the collector region of the gyrotron. Electrons move towards the analyzer through a slot in the collector, of 1 mm width and 40 mm in axial direction. To protect the analyzer from microwave field penetrating from HEB transport tunnel, a metal grid is installed immediately behind the slot, near the entrance of the analyzer pipe. Additional magnetic field is used to guide electrons to 1-mm input aperture of the analyzer. At the aperture position, the magnetic field is approximately 150 times weaker than at the maximum (plateau) of its distribution. For the working regime of the gyrotron, maximum current into analyzer did not exceed 1 mA.
The spherical analyzer utilizes the retarding-field method. Two versions of the analyzer with different shapes of the electrode under retarding potential were used (**Fig. 1**). In the first version (a) it is a spherical grid, and in the second (b) – a metal sphere with 10 mm – diameter aperture and a cone-shaped insert. Version (a) is characterized by a high degree of electric field uniformity, but secondary electrons emitted from the grid can, in principle, distort the real electron energy distribution. In version (b), electron bombardment of the electrode under the retarding potential is excluded. However, due to warping of electric lines, the energy resolution secured by this configuration is worse than for version (a).

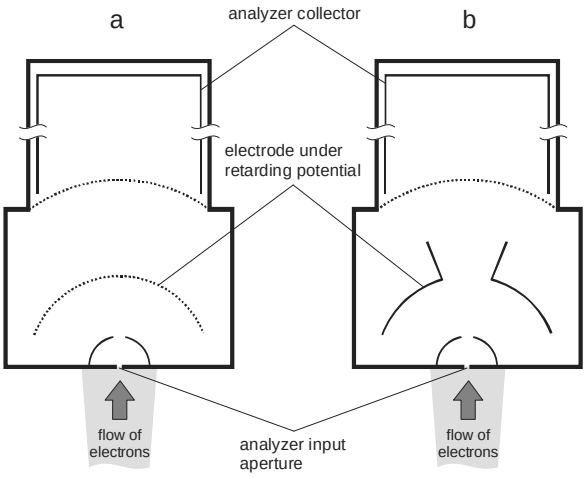

Fig. 1 Schematic drawing of the electron energy analyzer with the electrode under retarding potential in the form of a grid sphere (a) and metal sphere having aperture and special cone-shaped insert (b).

Two movable vacuum feedthroughs provide a possibility to displace the input aperture of the analyzer in transverse direction to the analyzed electron flow (and to measure energy spectra of electrons at different point of its cross-section), and to change the analyzer axis inclination to the direction of magnetic field lines. The latter possibility was used for correction of the analyzer position with respect to the H-lines. For suppression of interferences from the high-voltage pulse, the collector of the analyzer is shielded from the electrode under retarding potential by a metal grid (see Fig. 1).
The magnetic field in the analyzer region is relatively weak, so the transverse component of the electron velocity and the beam energy related to the transverse motion is negligible. Therefore the measured distribution corresponds to the distribution of the total beam energy.
In the experiments, the pulses of retarding voltage U_{ret} and analyzer current I_{an} are measured simultaneously. During a pulse, the U_{ret} value decreases slowly from the front that allows to obtain a cutoff curve during a single pulse of the gyrotron. The energy spectrum in the form of distribution function $f(\varepsilon)$ is obtained by differentiation of the measured dependence $I_{an}(U_{ret})$.

The electron energy is defined as $\varepsilon = eU_{\text{ret}}$. Out of this the relative root-mean-square value

$$\delta\varepsilon_{rms} = \frac{rms_{\varepsilon}}{\varepsilon_{mean}},$$

is obtained where

$$rms_{\varepsilon} = \sqrt{\int_{-\infty}^{+\infty} f(\varepsilon)\cdot(\varepsilon-\varepsilon_{mean})^2 d\varepsilon} \quad \text{and}$$

$$\varepsilon_{mean} = \int_{-\infty}^{+\infty} f(\varepsilon)\cdot\varepsilon\cdot d\varepsilon.$$

Yet, the retarding-potential method allows to obtain energy spread directly without any assumptions about the distribution function. In the references [11,12] the values of the retarding voltage $U_{\text{ret}(0.1)}$, $U_{\text{ret}(0.5)}$, $U_{\text{ret}(0.9)}$ are determined corresponding to the analyzer current reduction to 0.1, 0.5 and 0.9 of its maximum. The corresponding relative spread is then calculated as:

$$\delta\varepsilon_{0.1-0.9} = \frac{U_{ret(0.1)} - U_{ret(0.9)}}{U_{ret(0.5)}}.$$

Using this approach, we can estimate the spread as the width of the full spectrum excluding fractions of electrons with the highest and the lowest energies carrying 10 % of full current each. The ratio $\frac{\delta\varepsilon_{rms}}{\delta\varepsilon_{0.1-0.9}}$ depends on the shape of distribution $f(\varepsilon)$ and, for example, is equal to 0.39 for a Gaussian distribution.

Energy resolution, or minimum energy spread that can be registered by the analyzer, depends on its configuration. In the regimes with high magnetic field and low current, when the electron beam could be considered undisturbed, extremely narrow spectra were observed. Measured minimum values of energy spread $\delta\varepsilon_{0.1\text{-}0.9}$ were equal to 0.3 – 0.4 % for the analyzer version with grid electrode (a) and 0.6 – 0.8 % in the case of the analyzer with aperture and cone-shape insert (b) (see Fig. 1). Comparison of the data obtained with the two different analyzing systems shows that the spectra are characterized by approximately equal width in the presence of RF-fields caused by any type of space-charge instabilities. These data, as well as values of the width of the narrow spectra, give evidence of negligible influence of secondary electron emission from the grid in version (a) of the analyzer. Because of its higher sensitivity, it was used in the most part of measurements described below. When the data were obtained with version (b) it will be specially indicated. Achievement of high energy resolution ($\delta\varepsilon_{0.1\text{-}0.9}$ = 0.3 – 0.4 % corresponding to $\delta\varepsilon_{\text{rms}}$ = 0.1 – 0.15 %) allows to use this analyzer for study of the variation of the electron energy distribution under the action of non-stationary space-charge fields occurring at different stages of HEB instabilities development.

3 Experimental Results

Fig. 2a shows a typical electron energy spectrum measured in the regime with accelerating voltage U_0 = 28.2 kV, beam current I_b = 10 A, resonator magnetic field B_0 = 2.75 T and output power P_0 = 55 kW at the main $TE_{12,3}$ mode. The wide energy spread is due to the interaction of the electron beam with the RF-field in the resonator. For the shown spectrum, energy spread estimates are equal to $\delta\varepsilon_{0.1\text{-}0.9}$ = 103 % and $\delta\varepsilon_{\text{rms}}$ = 36 %. The measured spectra have been compared with the ones calculated in a self-consistent model [14] for the same values of operation parameters and different initial transverse velocity spread values $\delta v_{\perp\text{rms}}$. **Fig. 2b** gives the calculated spectrum for U_0 = 28.2 kV, I_b = 10 A, $\delta v_{\perp\text{rms}}$ = 10 % and velocity ratio (pitch-factor) $\alpha = v_{\perp}/v_{\parallel}$ = 1.1. The peaks on the low-energy side of this distribution originate from the simplified simulation of the continuous velocity distribution by only 5 groups of beamlets. In general, calculated spectra for velocity spread $\delta v_{\perp\text{rms}}$ = 5 – 15 % were in satisfactory agreement with the measured ones in the case of gyrotron resonator excitation at the main $TE_{12,3}$ mode.

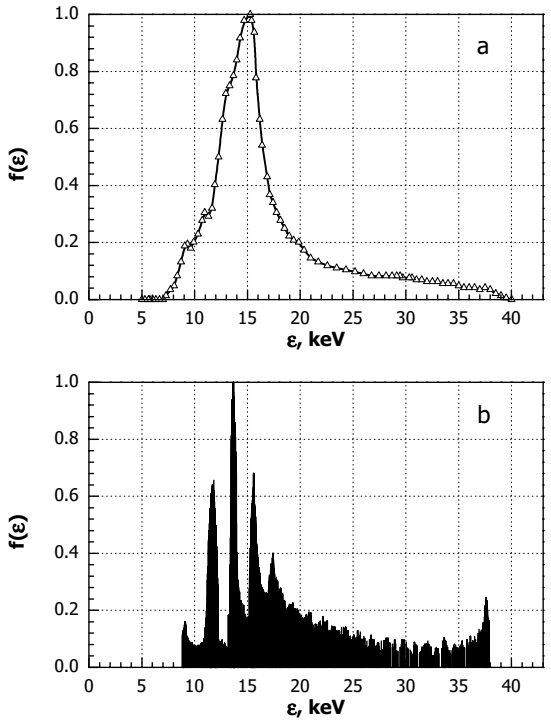

Fig. 2 Measured (a) and calculated (b) electron energy spectra (U_0 = 28.2 kV; I_b = 10 A; B_0 = 2.75 T; calculation for transverse velocity spread $\delta v_{\perp\text{rms}}$ = 10 % and pitch-factor α = 1.1).

As the experiment has shown, the electron energy spread was very small and limited only by the analyzer resolution, when the beam average pitch-factor $\alpha \leq 1$ and no RF-generation occurred. The values of α as well as velocity spread width and electron trajecto-

ries corresponding to all measurement regimes were calculated with the EGUN code. **Fig. 3** shows the plot of $\delta\varepsilon_{0.1\text{-}0.9}$ against the beam current I_b, measured in the regime with operating magnetic field B_0 = 2.75 T and reduced voltage U_0 = 16.8 kV. The spread value $\delta\varepsilon_{0.1\text{-}0.9} \cong 1$ % is practically constant over a broad interval of currents (in this measurement, the analyzer version with the metal sphere and aperture was used). It may be pointed out that, in the case of low pitch-factor, the electron beam is not disturbed by the RF-fields and no instability of any type develops, at least to the magnitude distinguishable by its contribution to the HEB energy spread.

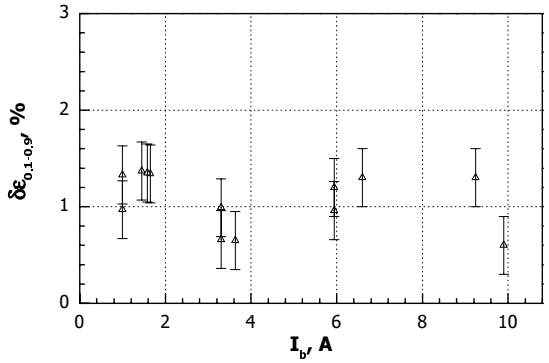

Fig. 3 Electron energy spread $\delta\varepsilon_{0.1\text{-}0.9}$ as a function of beam current I_b (U_0 = 16.8 kV; B_0 = 2.75 T; calculated pitch-factor α = 0.71 for I_b = 3.4 A).

Low-frequency signals associated with the development of instability of the space charge locked in the trap were registered in regimes with pitch-factor $\alpha >$ 1.1 – 1.2. In this case, we failed to avoid mm-wave radiation and thus obtained large broadening of energy distribution under the action of resonator RF-field for the wide range of voltages $7 \le U_0 \le 30$ kV. Moreover, this radiation existed not only for the standard gyrotron configuration but for the version with deinstalled resonator as well. In the latter case, the constant-diameter beam tunnel possibly acted as a microwave cavity.

Substantial suppression of mm-wave radiation was achieved by replacement of the resonator with the graphite RF-absorber. In the gyrotron with the absorber, measurements were performed at three values of voltage U_0 = 25.8, 16.8, 11.5 kV. For each of them, the beam current was chosen in agreement with the scaling relations ensuring conservation of electron trajectories [1,5,11]. The plots of the energy spread $\delta\varepsilon_{0.1\text{-}0.9}$ versus the plateau magnetic field B_0 for the given voltages are shown in **Fig. 4**. The dependencies of the calculated pitch-factor $\alpha(B_0)$ and the pulse-average amplitude of LFO signal obtained with the external antenna $A_{osc}(B_0)$ are also shown in the figure. In these experiments, the measured values of the LFO signal main spectral component were within the band 120 – 130 MHz. In Fig. 4, the energy spread $\delta\varepsilon_{0.1\text{-}0.9}$ abruptly increases from 0.3 – 0.4 % up to 4 – 8 % at a certain magnetic field value B_0. The LFO signals appear practically at the same value B_0 when the pitch-factor reaches the level of α = 1.1 – 1.2.

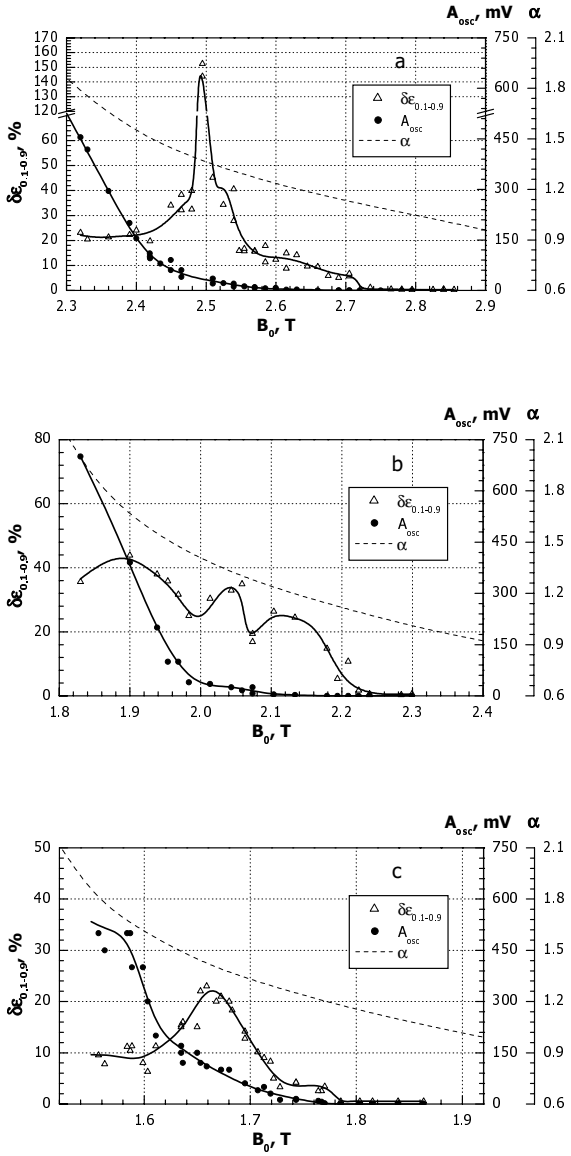

Fig. 4 Experimental gyrotron with graphite absorber: electron energy spread $\delta\varepsilon_{0.1\text{-}0.9}$, average amplitude of low-frequency oscillations A_{osc} and calculated pitch-factor α as functions of magnetic field B_0 (a – U_0 = 25.8 kV, I_b = 7.4 A; b – U_0 = 16.8 kV, I_b = 3.4 A; c – U_0 = 11.5 kV, I_b = 2.4 A).

Having fixed a voltage, we varied the beam current or magnetic field spatial distribution in the compression region. In both cases, the displacement of $\delta\varepsilon_{0.1\text{-}0.9}$ (B_0) and $A_{osc}(B_0)$ dependencies in the direction of larger or smaller B_0 values was correlated. The current increase stimulates reflection of electrons from the magnetic mirror due to the beam pitch-factor (and velocity spread) growth. As a result, appearance of the oscilla-

tions and sudden rise of energy spread take place at larger B_0 values.

Variation of the magnetic field distribution in the compression region does not change significantly the pitch-factor. However, it influences the development of instability of the space charge locked in the trap. Optimization of the magnetic field distribution, as it is shown in [13], can yield significant decrease of the LFO amplitude and increase of the threshold pitch-factor value corresponding to LFO appearance. In the present experiments for the voltage U_0 = 16.8 kV, the energy spread increased abruptly at $B_0 \cong 2.22$ T ($\alpha \cong 1.1$) for the standard magnetic field distribution and at $B_0 \cong 2.08$ T ($\alpha \cong 1.26$) for the optimized one. These data allow to suppose that RF-fields of bunched space charge in the trap are responsible for the electron energy spread, at least for magnetic fields (pitch-factors) near the threshold value.

While the LFO amplitude A_{osc} increases with reduction of the magnetic field B_0, the spread $\delta\varepsilon_{0.1\text{-}0.9}$ varies with B_0 non-monotonously (see Fig. 4a-c). Therefore in high-pitch-factor regimes, the electron energy spread can be associated with some sources different from the LFO. Unfortunately, even in the gyrotron with the RF-absorber, mm-wave radiation due to excitation of some cavity at cyclotron frequency remained one of such sources. For instance, radiation at a frequency f = 64 GHz was observed in the regime with U_0 = 25.8 kV and $B_0 \cong 2.5$ T together with extremely large energy spread (see Fig. 4a).

4 Numerical Simulation of Low-Frequency Oscillations in the Trap

Calculation of the influence of trapped space-charge on the electron energy spectrum was performed with a simplified PIC code simulating one-dimensional self-consistent movement of electrons in adiabatic approximation [15]. The code allows to determine the changes of electron energy under the action of large-scale (in comparison with the axial step of helical trajectory of a single electron) space-charge bunches oscillating in the trap. In the performed simulations the energy distribution of electrons passing to the magnetic field plateau region was calculated for different stages of LFO development. **Fig. 5** shows the plot of the beam potential U_b versus time t and the electron distributions on energy $f(\varepsilon)$ corresponding to different moments of time for the regime with operating values of the parameters U_0, I_b, B_0 and the transverse velocity spread $\delta v_{\perp rms}$ = 10 %. The dependence $U_b(t)$ was calculated in the cell situated at the end of the magnetic compression region at 18.9 cm distance from the cathode (the total length of magnetic compression region $z_{total} \cong 24$ cm). As shown in Fig. 5, accumulation of particles in the trap accompanies initial beam potential growth, whereupon oscillations at frequency $f \cong 125$ MHz develop. Increase of oscillation amplitude results in energy distribution broadening. For example, the moment of time t = 850 ns is characterized by the energy spread $\delta\varepsilon_{RMS}$ = 1.2 % ($\delta\varepsilon_{0.1\text{-}0.9}$ = 2.9 %). The data accumulated in the simulations show that the spread $\delta\varepsilon_{0.1\text{-}0.9}$ doesn't exceed 4 % even in regimes with the highest intensity of the oscillations.

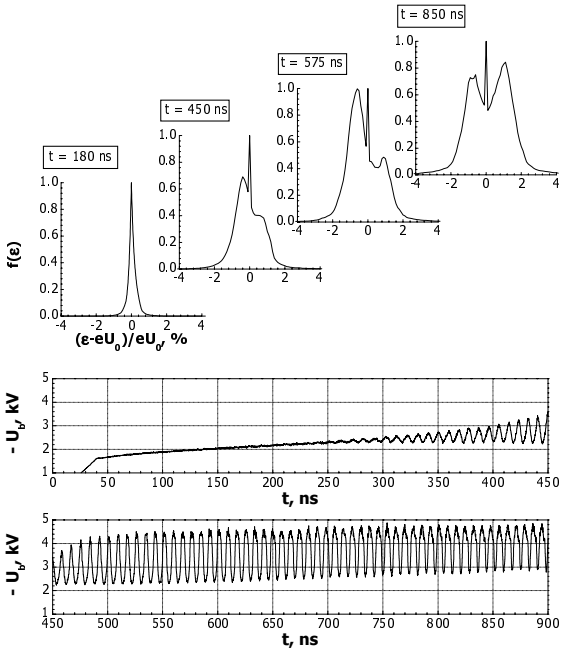

Fig. 5 Calculated beam potential U_b as a function of time t and electron energy spectra $f(\varepsilon)$ for different moments of time (U_0 = 30 kV; I_b = 10 A; B_0 = 2.75 T; transverse velocity spread $\delta v_{\perp rms}$ = 10 %).

5 Discussion of the Results and Conclusions

It can be concluded from the measurements in the gyrotron with the RF-absorber that the abrupt increase of electron energy spread at the pitch-factor $\alpha = 1.1 - 1.2$ can be caused by the development of parasitic low-frequency oscillations. However, the energy spreads measured in the presence of LFO significantly exceed the calculated values. This discrepancy can possibly be attributed to effects that could not be accounted for in these simplified calculations. The additional spread can result from 3D non-uniform shape of the electron bunches oscillating in the trap, associated with the specificity of HEB formation in the gyrotron electron-optical system including, for instance, cathode emission non-uniformity.

The non-monotonous character of $\delta\varepsilon_{0.1\text{-}0.9}(B_0)$ dependencies indicates the presence of other types of instabilities, not connected directly with the instability of space charge locked in the trap. These can be the negative-mass instability and the electron cyclotron

maser instability, both developing at the cyclotron frequency. Most likely, the latter was the cause of the mm-wave radiation at the frequency f = 64 GHz registered simultaneously with extremely large energy spread in the regime with U_0 = 25.8 kV and $B_0 \cong 2.5$ T. For other values of voltage and magnetic field, we didn't observe any signals in the frequency band covered by the 4-mm spectrum analyzer (54 – 80 GHz). In principle, both high-frequency instabilities can develop on the whole length of electron trajectories from the cathode to the collector. If this happens in the magnetic compression region where the cyclotron frequency is lower than that at the plateau, the radiation frequency can be below the spectrum analyzer band. Besides, due to quasi-electrostatic character of the negative-mass instability, it couples with external electrodynamic structures very weakly. As a result, its mm-wave field is difficult to register.

It wouldn't be correct to exclude from consideration other low-frequency instabilities that can be additionally stimulated by long-living electrons oscillating in the trap. For instance, the structure of RF-fields inherent to diochotron or double-stream low-frequency instabilities is characterized by small-scale non-uniformities. Therefore, their contribution to the total energy spread can be greater than calculated in Section 4.

In the experiments with the reduced voltage U_0 = 11.5 kV, the energy spread $\delta\varepsilon_{0.1\text{-}0.9}$ was approximately equal to 7 – 11 % for the region of low magnetic field $B_0 < 1.6$ T (see Fig. 4c), where the LFO signal amplitude is the highest. If we suppose the spread resulting from RF-fields to be caused by the trap instability, the measured values of the energy spread are 2 – 2.5 times greater that the calculated ones. In our opinion, taking into account approximate the character of the calculations such agreement is sufficiently good.

This work was supported by Forschungszentrum Karlsruhe (Germany) and by Russian Foundation for Basic Research.

6 Literature

[1] Dumbrajs, O.; Koponen, J.P.T.: Phys. Plasmas. Vol. 6, No. 6, 1999, pp. 2618-2621

[2] Avdoshin, E.G.; Goldenberg, A.L.: Radiophys. Quantum Electronics. Vol. 16, No. 10, 1973, pp. 1605-1612

[3] Kas'yanenko, D.V. et al.: Proc. Int. Workshop on Strong Microwaves in Plasmas: IAP, Nizhny Novgorod. Vol. 1, 2003, pp. 162-167

[4] Louksha, O.I.; Sominski, G.G.; Kas'yanenko, D.V.: J. Communications Technology and Electronics. Vol. 45, Suppl. 1, 2000, pp. 71-76

[5] Tsimring, Sh.E.: Int. J. Infrared Millimeter Waves. Vol. 22, No. 10, 2001, pp. 1433-1468

[6] Louksha, O.I.; Sominski, G.G.: Zh. Tekh. Fiz. Vol. 65, No. 2, 1995, pp. 198-202

[7] Bratman, V.L.: Zh. Tekh. Fiz. Vol. 46, No. 10, 1976, pp. 2030-2036

[8] Dumbrajs, O.; Nikkola, P.; Piosczyk, B.: Int. J. Electronics. Vol. 88, No. 2, 2001, pp. 215-224

[9] Bondeson, A.; Antonsen, T.M.: Int. J. Electronics. Vol. 61, No. 6, 1986, pp. 855-870

[10] Bratman, V.L. et al.: Zh. Tekh. Fiz. Vol. 70, No. 4, 2000, pp. 90-94

[11] Venediktov, N.P. et al.: Zh. Tech. Fiz. Vol. 70, No. 4, 2000, pp. 95-98

[12] Venediktov, N.P. et al.: Zh. Tech. Fiz. Vol. 70, No. 12, 2000, pp. 63-66

[13] Kas'yanenko, D.V. et al.: Radiophys. Quantum Electronics. 2004, to be published

[14] Borie, E: Computations of Radio-Frequency Behavior, Gyrotron Oscillators – Their Principles and Practice, C.J. Edgcombe, Ed. London, England: Taylor-Francis, 1993

[15] Borzenkov, D.V.; Louksha, O.I.: Zh. Tech. Fiz. Vol. 67, No. 9, 1997, pp. 98-101